ADVENGMAT
Vol. 25 – No. 14
July 2023

ADVANCED ENGINEERING MATERIALS

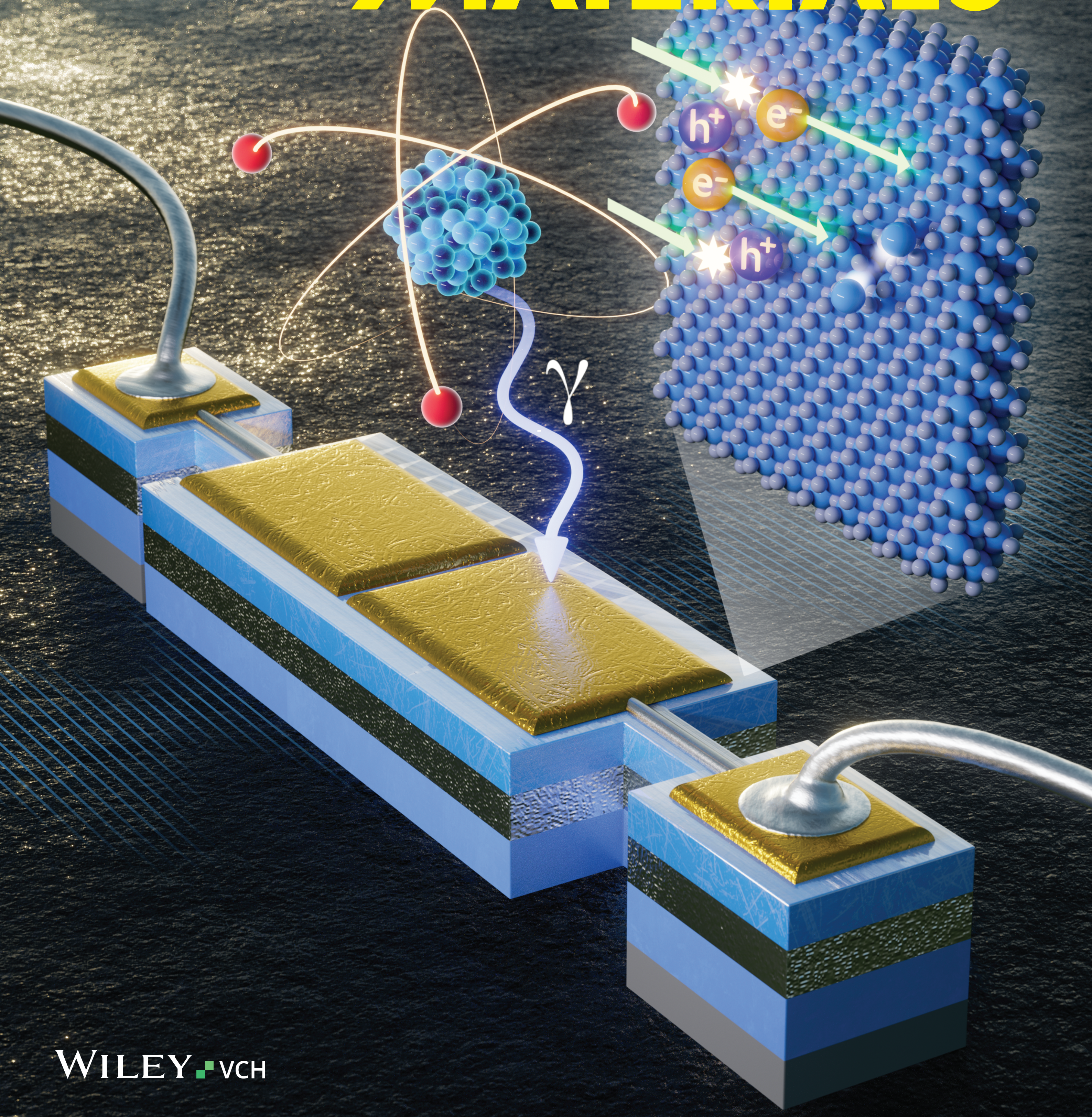

WILEY-VCH

Check for updates

Effects of Gamma Ray Radiation on the Performance of Microelectromechanical Resonators

David D. Lynes, Hengky Chandrahalim,* James E. Bevins, and James C. Petrosky*

While much radiation test data are available for metal-oxide-semiconductor (MOS) devices, research into the effects of radiation on microelectromechanical systems (MEMS) is in its relative infancy. Piezoelectrically transduced MEMS resonators have broad applications in signal processing, environmental monitoring, and navigation. Aluminum nitride (AlN), in particular, is an attractive piezoelectric because of its favorable fabrication characteristics and ease of integration into the complementary MOS (CMOS) manufacturing process. The utility of these devices in space and nuclear systems necessitates research into their performance in radiation environments. Resiliency and an established relationship between radiation dose and device behavior provide a critical tool for engineers in their design process. Multiple AlN-based MEMS resonator designs are created and exposed the devices to 1 Mrad(Si) gamma irradiation from a Cobalt-60 source while measuring scattering (S-) parameters in situ. The experimental data are matched to a theoretical model to describe the change in frequency as a function of radiation-induced displacement damage. It is demonstrated that the AlN-based resonators are resilient against radiation-induced charge-trapping effects. Furthermore, a new method is presented of permanent frequency trimming MEMS resonators up to 30% of their bandwidth without modifying quality factor or motional resistance.

1. Introduction

Gamma rays, emitted during atomic decay, are highly penetrative and necessitate substantial shielding for electronic devices. Shielding with 10 mm of lead attenuates gamma rays by only 10%.[1] Consequently, systems operating in high-gamma radiation environments often opt for lighter shielding. Co-60 sources, emitting gamma rays at an average energy of 1.25 MeV, serve as the standard for assessing ionization effects on electronics.[1,2] Notably, fission fuel and other radioactive structures in nuclear power plants emit gamma rays with an average energy of around 1 MeV, making Co-60 gamma rays suitable for simulating the electromagnetic environment of reactors.[1] In space missions, gamma rays themselves are not a significant radiation source. However, Co-60 gamma rays primarily generate Compton electrons, which effectively simulate penetrative electrons and protons in the space radiation spectrum.[1,2]

Extensive research has been conducted on radiation effects in metal-oxide-semiconductor (MOS) devices over the past 30 years.[3] In contrast, the study of radiation effects on microelectromechanical systems (MEMS) is still emerging. MEMS possess desirable characteristics such as low power consumption, lightweight design, small form factor, and potential integration with CMOS electronics, making them well-suited for space and other radiation-intensive applications.[4] While MOS devices are often identified as the weak link in electronic system reliability within radiation environments, advancements in gate size reduction, processing techniques, and alternative dielectrics have significantly enhanced their reliability.[3,5,6] MEMS serve as enabling technologies in various scientific applications, such as the atomic force microscope (AFM) sensor for the Mars Phoenix Mission, gyroscopes, accelerometers, and star-tracking cameras for microsatellites,[7–10] and vibration sensors deployed on nuclear power plant structures.[4,7–12] Consequently, it is crucial to carefully evaluate the performance of MEMS in diverse radiation environments to mitigate potential failure risks, despite their previous "rad-hard" reputation.

Piezoelectrically transduced MEMS find widespread use in diverse applications, including energy harvesting, signal processing, robotics, aerospace, and defense.[11,13–22] Compared to alternative transduction methods like thermal/piezoresistive, capacitive, and electrostatic schemes, piezoelectric materials offer advantages such as higher energy density, superior frequency scaling, lower power configurations, and easier characterization and integration.[23–33] Incorporating additives into piezoelectric materials enhances material constants and aging characteristics.[34] Particularly, microscale resonant devices

D. D. Lynes, H. Chandrahalim
Department of Electrical and Computer Engineering
Air Force Institute of Technology
Wright-Patterson Air Force Base, OH 45433, USA
E-mail: david.lynes.2@us.af.mil; hengky@microsystems.group

J. E. Bevins, J. C. Petrosky
Department of Engineering Physics
Air Force Institute of Technology
Wright-Patterson Air Force Base, OH 45433, USA

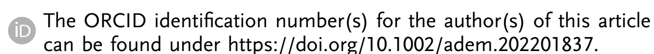
The ORCID identification number(s) for the author(s) of this article can be found under https://doi.org/10.1002/adem.202201837.

© Published 2023. This article is a U.S. Government work and is in the public domain in the USA. Advanced Engineering Materials published by Wiley-VCH GmbH. This is an open access article under the terms of the Creative Commons Attribution-NonCommercial License, which permits use, distribution and reproduction in any medium, provided the original work is properly cited and is not used for commercial purposes.

DOI: 10.1002/adem.202201837

15272648, 2023, 14, Downloaded from https://onlinelibrary.wiley.com/doi/10.1002/adem.202201837, Wiley Online Library on [18/07/2023]. See the Terms and Conditions (https://onlinelibrary.wiley.com/terms-and-conditions) on Wiley Online Library for rules of use; OA articles are governed by the applicable Creative Commons License

utilizing piezoelectric transduction, known as piezo-MEMS resonators, find extensive utility in inertial sensing, radio frequency (RF) signal processing, and environmental monitoring applications.[35–47] They serve as filters, sensors, and clock generators,[48] offering high selectivity, narrow bandwidth, and good stability.[34] These characteristics, along with their ongoing miniaturization, affordability, and compatibility with CMOS technology, position piezo-MEMS resonators as excellent choices for deployment in microsatellites and radiation monitoring systems.

Aluminum nitride (AlN) is an excellent piezoelectric material for MEMS resonators. AlN thin films retain most of their bulk physical, thermal, and electric properties, making them highly desirable. The sputtering deposition of AlN requires low temperatures (<400 °C), making it compatible with CMOS integration.[49–54] Moreover, AlN does not introduce contamination to the cleanroom environment and can be doped to enhance electromechanical coupling while maintaining a high quality (Q) factor.[49,55] AlN has been successfully utilized as a transducer in numerous applications, including energy harvesters, acoustic devices, sensors, actuators, RF filters, and accelerometers.[11,49,56,57]

The broad utility and practicality of AlN-based piezo-MEMS resonators make them well-suited for use in devices that may encounter harsh radiation environments. Thus, the importance of characterizing radiation effects in piezo-MEMS resonators is twofold: 1) High Q resonators are designed for high signal sensitivity and resolution. The extremely narrow bandwidth required of these devices makes them vulnerable to shifts in performance due to radiation-induced degradation; and 2) Increasing loss weakens the signal for RF processing or reduces output power in energy harvesting applications. Low-loss resonators are also vulnerable in signal processing and energy harvesting applications. Therefore, this work investigates the effects of ionizing radiation on AlN-based MEMS resonators.

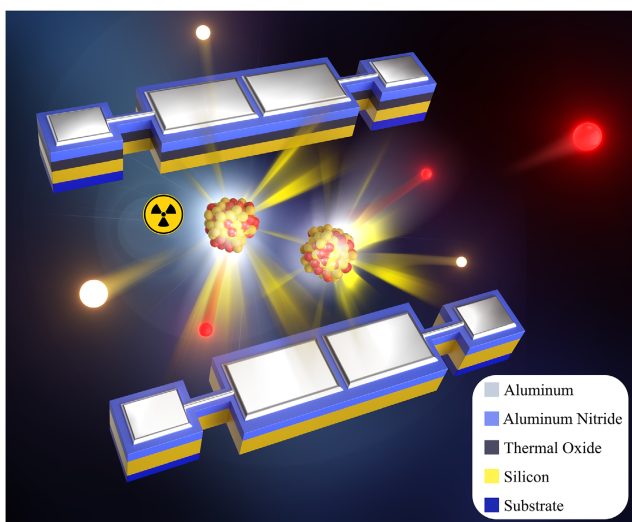

Figure 1. Illustration of AlN transduced two-port rectangular flat plate resonators. Two resonator designs were irradiated: one with SiO_2 thin film (top) and one without (bottom). The devices were irradiated using the OSU Co-60 Underwater Irradiator. S-parameters were measured in situ to develop empirical models of device behavior while in an ionizing radiation environment.

This work explores how the effects on the resonator change when a thin film dielectric layer is added to the device design. AlN transduced two-port rectangular flat plate resonators with and without a silicon dioxide (SiO_2) thin film (**Figure 1**) were designed and commercially fabricated. The devices were mounted to a custom printed circuit board (PCB) and exposed to 1 Mrad(Si) using The Ohio State University's (OSU) Cobalt-60 (Co-60) Underwater Irradiator. During irradiation, scattering (S-) parameters were measured in situ. Measured resonant frequency, motional resistance, quality factor, and one-port electromechanical coupling are used to validate a theoretical model that describes the device reaction to the total dose effects of atomic displacement damage and charge generation/trapping. This work also presents a new method of permanent frequency trimming MEMS resonators by up to 30% of their bandwidth without modifying quality factor or motional resistance.

2. Results and Discussion

2.1. Background

The initial interaction of Co-60 gamma rays with solid matter is Compton scattering.[58] The direct result of the Compton interaction is the ionization of an electron and the scattering of a lower energy X-ray. These electrons and photons continue interacting within the material, creating a cascade that can generate hundreds to thousands of electron–hole pairs (EHP).[1] Most electrons immediately recombine with the holes. The electrons and holes that escape this initial recombination usually recombine as they drift through the material. Some fraction of the free holes and electrons are trapped. For instance, it has been shown in SiO_2 that the trapping of holes causes a positive oxide-trap charge.[1] Also, the hydrogen ions freed during the hole "hopping" process may drift to the SiO_2-Si interface to form positive interface traps.[1] Similarly, researchers have shown that electrons can be trapped in the bulk of a dielectric and at its interfaces, forming regions of negative bias.[59,60]

In addition to creating EHPs, the secondary electrons released from high-energy gamma rays, like those from Co-60, may have sufficient energy to displace atoms. Silicon (Si) irradiation by gamma rays can produce Compton electrons in the energy range of 0.1–0.9 MeV; the electron threshold energy required to cause a displacement in Si has been reported between 0.125 and 0.145 MeV.[1] In turn, the electron-displaced Si atoms can receive enough energy to displace other Si atoms or ionize other electrons. The direct result is that the gamma radiation produces vacant lattice sites in Si, and the displaced atoms will come to rest as interstitials. The number of displacements per unit volume (N_d) caused by energetic electrons in a solid is given by

$$N_{\mathrm{d}} = n_{\mathrm{a}} \sigma \overline{\upsilon} \Phi \tag{1}$$

where n_a is the number of atoms per unit volume of the absorber (5×10^{22} Si atoms cm^{-3}), σ is the energy-dependent displacement cross section (68×10^{-24} cm^{-2} for 1 MeV electrons in Si), $\overline{\upsilon}$ is the average displacement per primary displacement, and Φ is the radiation fluence.[61] Previous research has shown that for n-type silicon (n-Si), the displacements caused by a total dose of 1 Mrad(Si) of Co-60 gamma irradiation is equivalent to

© Published 2023. This article is a U.S. Government work and is in the public domain in the USA. Advanced Engineering Materials published by Wiley-VCH GmbH

15272648, 2023, 14, Downloaded from https://onlinelibrary.wiley.com/doi/10.1002/adem.202201837, Wiley Online Library on [18/07/2023]. See the Terms and Conditions (https://onlinelibrary.wiley.com/terms-and-conditions) on Wiley Online Library for rules of use; OA articles are governed by the applicable Creative Commons License

that caused by a fluence of 1.25×10^{13} cm^{-2} 1 MeV electrons.[62] Furthermore, the model created by Kinchin and Pease predicts that the average number of displacements in Si is 1.53 per 1 MeV electron.[61,63] From Equation (1), it is possible to predict approximately 6.5×10^{13} displacements cm^{-3} in the Si from 1 Mrad(Si) Co-60 gamma rays.

The atomic displacements caused by the high-energy Compton electrons result in interstitial and vacancy defects. The displacements slowly increase the material's disorder. That is, there is a change from high long-range order to high long-range disorder. On a bulk scale, crystalline materials have different elastic moduli than their amorphous counterparts. For example, crystalline silicon has an elastic modulus, C_{11} of approximately 169 GPa, whereas amorphous silicon has an elastic modulus of roughly 80 GPa.[64,65] Furthermore, the transition from high order to high disorder decreases the atomic packing factor and, in turn, decreases the mass density of the material. Using silicon as an example again, crystalline silicon's density is greater than amorphous silicon's ($2.328\ g\ cm^{-3}$ vs $2.285\ g\ cm^{-3}$).[66] Additionally, as the mass density changes, the device dimensions change. At some point, equilibrium is reached when the number of displacements occurring no longer increases the long-range order of the material.

The time rate of change of atomic displacements in a crystalline solid is proportional to the dose rate, φ, by a constant, κ, that represents the number of displacements that occur per unit dose

$$\frac{dD(t)}{dt} = \kappa\varphi. \tag{2}$$

The proportionality constant, κ, depends on how many displacements exist. Therefore, κ is modified by the ratio between the number of current atomic displacements, $D(t)$, and the number of displacements that exist as the dose goes to infinity, D_{sat}

$$\frac{dD(t)}{dt} = \kappa\left(1 - \frac{D(t)}{D_{sat}}\right)\varphi \tag{3}$$

Assuming an initial preirradiation displacement density, D_o, the solution to this first-order linear differential equation is

$$D(t) = (D_o - D_{sat})e^{-\frac{\kappa\varphi}{D_{sat}}t} + D_{sat} \tag{4}$$

If φ is constant throughout the exposure, the product φt now represents the total dose, Φ, such that

$$D(\Phi) = (D_o - D_{sat})e^{-\frac{\kappa}{D_{sat}}\Phi} + D_{sat} \tag{5}$$

Other work has shown that Young's modulus of a material is representable as a linear relationship to the crystallinity of a solid.[67,68] That is

$$E(\Phi) = mD(\Phi) + b \tag{6}$$

where m and b are constant and real. In this case, the constants m and b are not known, so it is more helpful to look at the fractional change to Young's modulus. The fractional change to Young's modulus is the ratio between Young's modulus at some fluence, $E(\Phi)$, and the preirradiation Young's modulus, E_o, such that

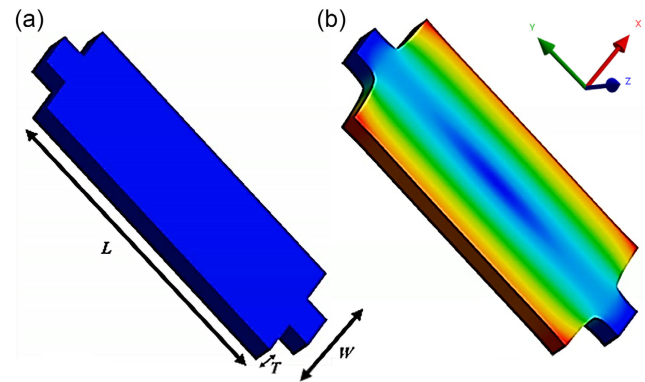

Figure 2. a) An example of a two-anchor rectangular flat plate resonator and its critical dimensions. b) An example of the motion of the 1st (fundamental) WEM vibration.

$$\frac{E(\Phi)}{E_o} = (1 - A)e^{-\frac{\Phi}{\tau}} + A \tag{7}$$

where $\tau = D_{sat}/\kappa$ and $A = E_{sat}/E_o$.

The device used to test the gamma-ray effects on piezo-MEMS resonators was a two-port two-anchor rectangular flat plate resonator, as shown in **Figure 2**a. The radiation response of the fundamental width extensional mode (WEM) was explored in this work. The equations of motion of the first WEM can be solved analytically. The first WEM is also one of the strongest resonance modes exhibited by this geometry. The WEM resonant vibration is achieved when an in-plane longitudinal standing wave is formed along the width of the rectangular plate. An example of the first WEM's vibrational motion is shown in Figure 2b. The resonant frequency, f_r, of the first WEM, is described by

$$f_r = \frac{1}{2W}\sqrt{\frac{E_{eff}}{\rho_{eff}}} \tag{8}$$

where W is the width of the resonator as shown in Figure 2a and E_{eff} and ρ_{eff} are the effective Young's modulus effective mass density of the material stack, respectively.[21,46]

The small signal equivalent circuit components—motional resistance (R_m), capacitance (C_m), and inductance (L_m)—have been derived in previous work.[40] Specific to this research, the analytical solution of R_m for a two-port piezoelectrically transduced resonator built on a substrate operating in the fundamental WEM is given by

$$R_m = \frac{\pi}{4}\frac{T}{L}\frac{\sqrt{E_{eff}\rho_{eff}}}{QE_{iezo}^2 d_{31}^2} \tag{9}$$

where T is the total thickness of the resonator, L is its length, and d_{31} is the transverse piezoelectric coefficient.[69] E_{piezo} and ρ_{piezo} are Young's modulus and the effective mass density of the piezoelectric layer, respectively. The quality factor (Q) measures how damped the resonator is. In another sense, Q is a measure of efficiency and energy loss. Q is comprised of several different loss mechanisms, such as mechanical, electrical, and material losses.[21,46] For this experiment, we mathematically describe Q as

 © Published 2023. This article is a U.S. Government work and is in the public domain in the USA. Advanced Engineering Materials published by Wiley-VCH GmbH

$$\frac{1}{Q} = \frac{1}{Q_o} + \frac{1}{Q_{trap}} + \frac{1}{Q_{disp}} \quad (10)$$

where Q_o represents the mechanisms not affected by radiation such as an anchor or fluidic losses, Q_{trap} represents all loss mechanisms that may be affected by trapped charges due to radiation such as dielectric loss, and Q_{disp} is associated with loss mechanisms affected by displacement damage such as mechanical and material losses. Other sources of loss, such as thermoelastic damping (TED) and squeeze film damping, hold minimal significance. TED pertains to the phenomenon of phonon diffusion from regions of higher temperature to lower temperature areas. In the frequency range of operation for the devices in this study, TED's impact on bulk-mode resonators is considered negligible.[70–72] Similarly, squeeze film damping can be deemed negligible due to the absence of small air gaps surrounding the resonator. From Equation (8)–(10) charge generation and trapping have an effect on Q and, in turn, R_m. Notably, f_r is independent of the effects of charge trapping. In contrast, displacement damage will affect Q, d_{31}, E_{eff}, and E_{piezo}. Therefore, it is reasonable to expect changes to both R_m and f_r due to displacement damage.

The Young's modulus of the material is not directly measurable from the resonator's frequency response, but the resonant frequency, f_r, can be. As previously discussed, as the crystal is amorphized, the changes to device dimensions and mass density are negligible compared to the change to material elasticity.[64–66] Therefore, using Equation (8), the fractional change to resonant frequency can be written as

$$\frac{f_r(\Phi)}{f_{r_o}} = \sqrt{\frac{E_{eff}(\Phi)}{E_{eff_o}}} \quad (11)$$

where f_{r_o} is the initial, preirradiation, resonant frequency.

From Equation (1), it was shown that 1 Mrad(Si) only displaces approximately 1 in every 1 billion atoms. In other words, there is only a slight increase in atomic displacement density. Therefore, the value $E_{eff}(\Phi)/E_{eff_o}$ is assumed to be very close to unity. In this case, it is possible to approximate Equation (11) with a first-order Taylor expansion. That is, $\sqrt{x}_{x\approx 1} \approx \frac{x}{2} + \frac{1}{2}$. And so, the fractional change to resonant frequency can now be written as

$$\frac{f_r(\Phi)}{f_{r_o}} = (1-\alpha)e^{-\frac{\Phi}{\tau}} + \alpha \quad (12)$$

where $\tau = D_{sat}/\kappa$ and $\alpha = f_{r_{sat}}/f_{r_o} \approx \sqrt{E_{eff_{sat}}/E_{eff_o}}$.

2.2. Experiment

The devices under test are two-port two-anchor AlN transduced rectangular flat plate MEMS resonators. From bottom to top, the resonators consist of a 10 µm thick n-doped silicon layer, an optional 0.2 µm thick SiO_2 thin film, a 0.5 µm AlN layer, and a 1.02 µm Al/Cr electrode layer. The devices are fabricated on a silicon-on-insulator (SOI) handle wafer by MEMSCAP, Inc. The Supporting Information section presents details regarding MEMSCAP's PiezoMUMPs fabrication process. We designed devices with and without the SiO_2 layer such that the top electrode and AlN layers were identical. The device dimensions and material properties are presented in **Table 1**. To prepare the resonators for irradiation, the devices were diced and glued to a custom PCB using conductive silver paste. Wirebonds for ground and signal connections were made using 99% gold 1-mil bonding wires. 50 Ω SMA connectors were soldered to the PCB to provide the RF connection during irradiation. **Figure 3** presents (a) cross-sectional scanning electron microscope (SEM) images of aluminum nitride transduced MEMS resonator designs, with and without a SiO2 thin film, (b) and (c) SEM images of a device before and after gluing and wire bonding, and (d) a final prepared package. It should be noted that the AlN transducer layer was deposited during the same fabrication step for both resonators, with and without the oxide layer. However, the device incorporating the oxide layer demonstrates the presence of finer columnar features, as shown in Figure 3a.

The irradiation was conducted at the Co-60 Underwater Irradiator at The Ohio State University. The Co-60 sources are kept in a 16 ft deep pool at OSU's facility. A 6 inch diameter dry access tube allowed the devices to be lowered next to the sources for uniform exposure at the maximum possible dose rate. The dry tube's diameter permitted the irradiation of two resonators simultaneously. Twenty-five feet LMR-240 coax cables connected the devices to the VNAs. VNA RF input power was 0 dBm. Before lowering the devices into the dry-tube, two-port short-open-load-through (SOLT) was accomplished to correct line error. S-parameters were continuously recorded in situ during irradiation and for a 15 min postirradiation timed anneal. Total six devices were irradiated (3 with and 3 without the SiO_2 thin film) to a total dose of 1 Mrad(Si). The Co-60 irradiator was originally calibrated in 2002. The dose rate was revalidated in 2016 by irradiating Landauer nanoDot dosimeters for 10 and 40 min. Based on the previous calibration and the half-life of Co-60, the dose rate at the time of the experiment was approximately 12.8 krad h^{-1}. The devices were irradiated at atmospheric pressure and room temperature. A diagram of the experimental setup is presented in **Figure 4**.

Table 1. Layer dimensions and bulk material Properties.

Parameter	Al	AlN	SiO_2	n-Si
Dimensions (No SiO_2 layer) $L \times W \times T$ in [µm]	97 × 37 × 1.02	206 × 46 × 0.5	Not applicable	216 × 56 × 10
Dimensions (With SiO_2 layer) $L \times W \times T$ in [µm]	97 × 37 × 1.02	206 × 46 × 0.5	216 × 56 × 0.2	222 × 62 × 10
Density [kg m^{-3}]	2,700	3,260	2,465	2,330
Young's modulus [GPa]	69	325	70	166

© Published 2023. This article is a U.S. Government work and is in the public domain in the USA. Advanced Engineering Materials published by Wiley-VCH GmbH

15272648, 2023, 14, Downloaded from https://onlinelibrary.wiley.com/doi/10.1002/adem.202201837, Wiley Online Library on [18/07/2023]. See the Terms and Conditions (https://onlinelibrary.wiley.com/terms-and-conditions) on Wiley Online Library for rules of use; OA articles are governed by the applicable Creative Commons License

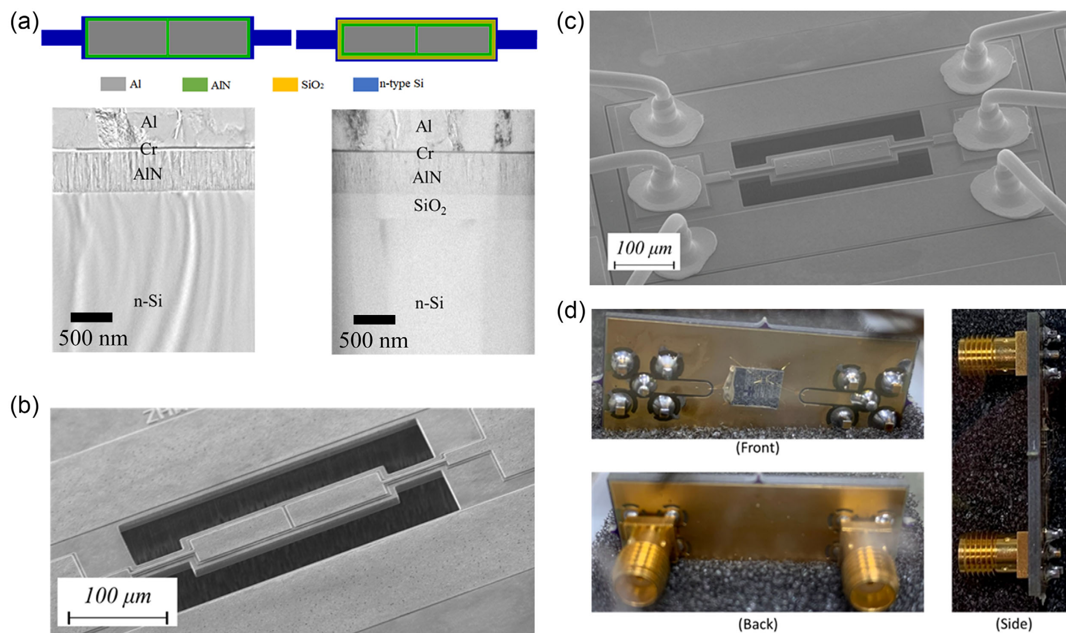

Figure 3. a) Cross-sectional SEM images of aluminum nitride transduced MEMS resonator designs, with and without SiO_2 thin film. b) SEM image of a device after fabrication (no SiO_2). c) SEM image of a device after gluing and wire bonding to PCB (with 0.2 μm SiO_2). d) Example of a final device prepared for irradiation.

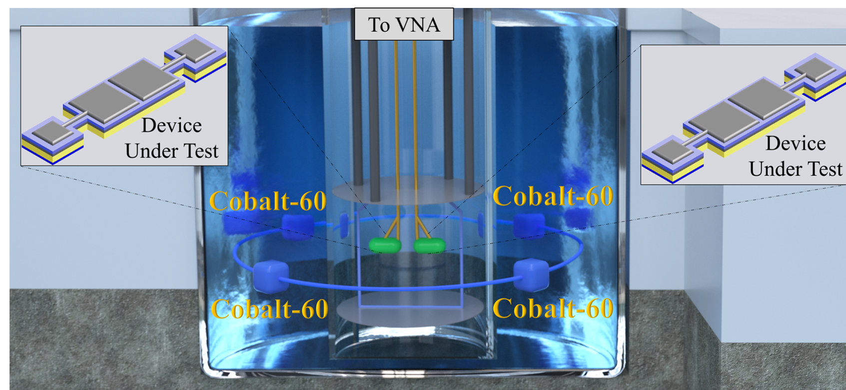

Figure 4. Diagram of The Ohio State University's Co-60 Underwater Irradiator (not to scale). The pool is nearly 16 feet deep. Two devices were irradiated simultaneously by lowering them next to the Co-60 sources via a dry access tube. Coax cables led out of the dry access tube to VNAs (not pictured) that continuously recorded S21 and S11 parameters for both devices during irradiation.

2.3. Results

S-parameter data were postprocessed to determine f_r, Q, R_m, and one-port effective electromechanical factor (k^2_{eff}). Q, R_m, and one-port k^2_{eff} were calculated in the usual manner for two- and one-port resonators presented by Bhugra and Piazza and Wu et al.[21,46,73]

Figure 5 presents the frequency response from two different resonators under irradiation, one without the 0.2 μm oxide layer (a) and one with the additional layer (b). IL and Q change very little throughout the exposure. f_r exhibits a small but significant trimming during irradiation. The magnitude of the frequency trim of the device with the 0.2 μm oxide layer is roughly half that of the resonator without the additional layer. The ≈50% difference in frequency trim magnitude is consistent across all devices tested. Raman spectra of pre- and postirradiated silicon were collected to assess the change in crystallinity. Results are presented in the Supporting Information. No detectable change in crystallinity was measured. The gamma irradiation has not amorphized the crystalline structures of the device, but sufficient displacements have been introduced to change its behavior.

In both devices, there is frequency trimming. The magnitude of the frequency trimming for the device with the oxide layer is approximately half that of the resonator without the SiO_2 layer. Color warmth increases with total dose.

© Published 2023. This article is a U.S. Government work and is in the public domain in the USA. Advanced Engineering Materials published by Wiley-VCH GmbH

15272648, 2023, 14, Downloaded from https://onlinelibrary.wiley.com/doi/10.1002/adem.202201837, Wiley Online Library on [18/07/2023]. See the Terms and Conditions (https://onlinelibrary.wiley.com/terms-and-conditions) on Wiley Online Library for rules of use; OA articles are governed by the applicable Creative Commons License

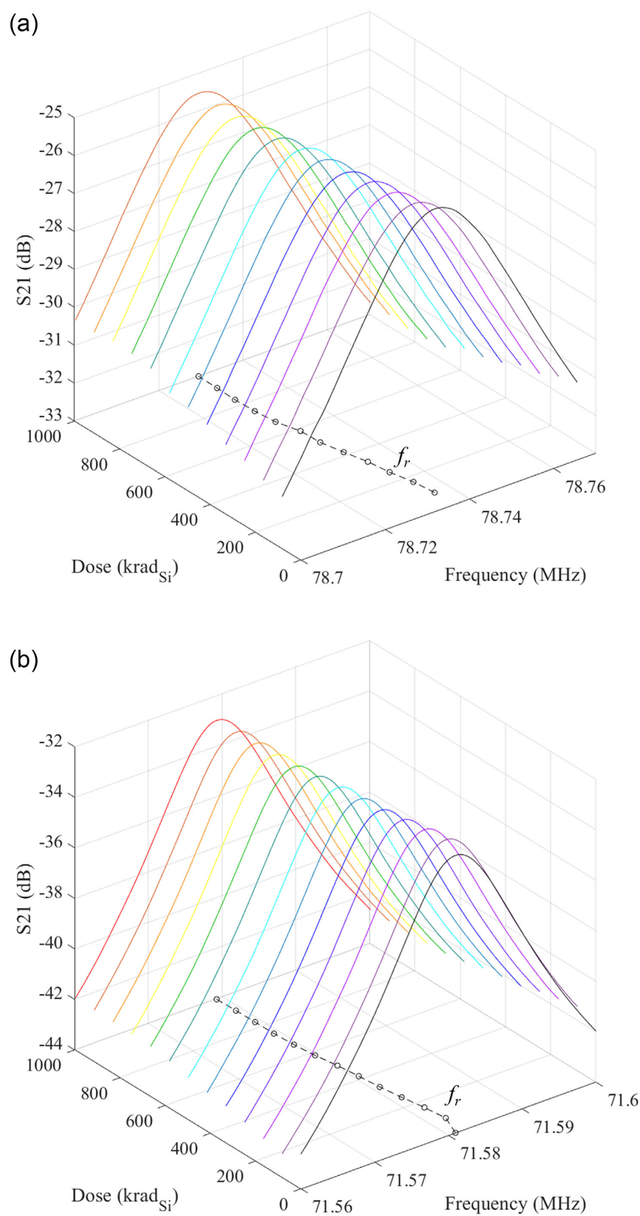

Figure 5. Measured frequency response during gamma irradiation for a) a device without the SiO_2 thin film and b) a device with the 0.2 μm SiO_2 layer.

The measured values of f_r, Q, R_m, and one-port k^2_{eff} pre- and post-1 Mrad(Si) gamma irradiation are tabulated in the Supporting Information section. The reduction in resonant frequency after the 1 Mrad(Si) exposure is consistent across all irradiated devices. Q, R_m, and k^2_{eff} do not have a consistent or significant pattern of change from the irradiation. The observed changes in f_r from irradiation are significantly smaller than the differences between devices due to fabrication imperfections. The magnitude of the measured frequency shifts is 10% to 30% of the resonator's bandwidth. **Figure 6** presents the fractional shift (e.g., $1 - f_r(\Phi)/f_{r_o}$) for the in situ measurements of f_r, Q, R_m, and k^2_{eff} for both resonator designs. Here, we see f_r gradually decreases with increasing total dose for both devices. Q, R_m, and k^2_{eff} experience fluctuations that are not consistent between devices and are, ultimately, relatively stable throughout the gamma irradiation. The resonant frequency of the devices with the thin film dielectric shifts an average of 37.5 ppm after 1 Mrad(Si), whereas the f_r of the devices without a SiO_2 layer shift an average of 60.0 ppm, nearly double.

A 15 min room temperature timed anneal was performed immediately after gamma irradiation. Table S2 in the Supporting Information section presents the measured values of f_r, Q, R_m, and k^2_{eff} after the time anneal. There is no significant shift to any resonator parameters after the timed anneal. Therefore, the frequency shift caused by the gamma irradiation is stable at room temperature.

2.4. Discussion

A statistical analysis was conducted on the data to illustrate the significance of the resonant frequency shift. The data were graphically presented in **Figure 7**, depicting the mean and standard deviation, for both sets of devices: three with the oxide layer (Figure 7a) and three without the oxide layer (Figure 7b). Notably, the six devices (three with the SiO_2 thin film and three without) underwent irradiation in three distinct experimental runs, accumulating a total dose of 1 Mrad(Si). The observed frequency exhibits a consistent decrease after each experimental run. These deviations are statistically significant, thereby asserting the influence of an unaccounted-for factor. Given the consistency of this shift across both device designs, it can be inferred that this factor is a common element. The shift is consistent across both device designs; therefore, it is a common factor. The magnitude of the shift from the first to the third run of 40–50% does not correlate with the nuclear decay of Co-60. With a half-life of 5.27 years, the activity of the Co-60 decreased only 0.75% during the 3-week experimentation period. The shifts are most likely attributable to the imprecision of device placement inside the dry tube. The ideal placement of the devices is level with the Co-60 sources at a radius of 2.5 inches. An error in elevator height of only 2 inch can decrease the dose rate by almost 50%. The error is not sufficiently significant to reject the results, as demonstrated by the *t*-tests.

Assuming a *t*-distribution for a small sample size, all data are within three standard deviations, $3S$, of the mean; therefore, no data are rejected as outliers. Using a null hypothesis of no change (i.e., $h = 0$) and applying the one-tailed *t*-test, there is a 98.2% confidence that the frequency shift for the device with the oxide layer (blue) is statistically significant. There is a 96.4% confidence for the device without the oxide layer (red) that the shift is significant. The frequency shift between device designs was compared using the two-sample *t*-test. The resulting *P*-value is 0.30. Using the conventional significance level of 0.05, it cannot be concluded that the added SiO_2 creates a significant difference in how the device's resonant frequency changes when exposed to gamma rays.[74] Overall, a small but significant shift in resonant frequency is present during gamma irradiation up to 1 Mrad(Si) for both device designs.

Recognizing that, by Equation (8), the resonant frequency of a WEM device is independent of electric fields, and gamma

© Published 2023. This article is a U.S. Government work and is in the public domain in the USA. Advanced Engineering Materials published by Wiley-VCH GmbH

15272648, 2023, 14, Downloaded from https://onlinelibrary.wiley.com/doi/10.1002/adem.202201837, Wiley Online Library on [18/07/2023]. See the Terms and Conditions (https://onlinelibrary.wiley.com/terms-and-conditions) on Wiley Online Library for rules of use; OA articles are governed by the applicable Creative Commons License

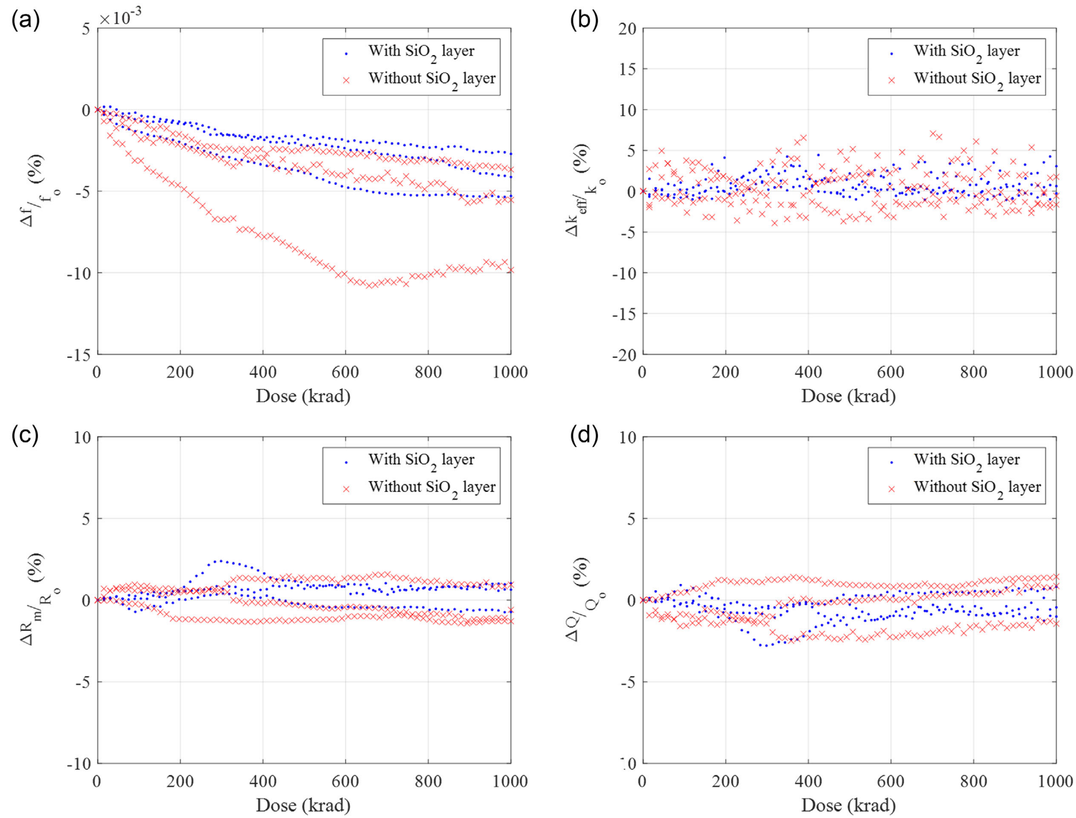

Figure 6. Measured fractional change to resonator parameters during exposure to 1 Mrad(Si). Shown are the a) f_r, b) one port k_{eff}^2, c) R_m, and d) Q for six different resonators while being exposed to 1 Mrad(Si) Co-60 gamma irradiation. Three of the devices had a SiO_2 thin film between the AlN and n-Si layers (blue) and three did not (red).

irradiation does not add material, the source of the frequency trimming is the gamma radiation causing small amounts of localized displacement damage. As previously discussed, the difference in stiffness between crystalline and fully amorphous Si is much more significant than the difference in mass densities.[64–66] From this, it can be concluded that any change in device dimensions is negligible, and gamma irradiation primarily alters the acoustic velocity of the material. From Equation (8), the acoustic velocity values pre- and postirradiation are extracted. These data are presented in **Table 2**. In addition to the measured changes in f_r, Q is not altered significantly after the 1 Mrad dose. By Equation (10), the Q of the device is dominated by Q_o. In other words, the loss factors that dominate the Q of the resonator are unaffected by gamma irradiation, at least up to 1 Mrad.

The gamma interactions can be considered uniform throughout the device. Therefore, the displacements in the AlN layer should decrease d_{31}. However, R_m does not have a statistically significant change, implying d_{31} does not change significantly for this radiation dose. Noting that Q remains unchanged, then by Equation (9) R_m is proportional to $\sqrt{E_{eff}\rho_{eff}}$. A reduction in the effective Young's modulus, and thus a reduction in acoustic velocity (as demonstrated by the shift in f_r), should decrease R_m. However, this amounts to only tenths of Ohms in difference, significantly below the noise threshold of the measurement setup, as shown in the right-most column of **Table 2**.

Finally, the measured fractional shift to f_r is fit to Equation (12) from the decaying exponential model to determine τ and α for both device designs. The results are shown in **Figure 8**. The decay constant, τ, depends on device design and radiation type. The decay constant, τ, is shorter for the device without the added SiO_2 layer. That is, the device reaches equilibrium more quickly. The shorter τ is attributable to the addition of the oxide thin film. The SiO_2 layer is amorphous, and the displacement energy for oxygen is almost twice that of silicon. Therefore, the SiO_2 layer is less susceptible to changes due to displacement damage, making the device less susceptible to change from gamma irradiation. So, it is reasonable that τ is higher for the device with the added oxide layer.

Previous work has shown that this device design is susceptible to thermal effects. Additionally, localized thermal spikes from the irradiation may also cause the depoling of AlN. The thermal effects on these devices are reversible without hysteresis.[70] Furthermore, AlN is essentially immune to thermal spike damage, and the thermal spikes are not above the melting temperature of Si.[75] This experiment's statistically significant frequency trim remains unchanged after a 15 min postirradiation time anneal. Therefore, displacement damage is likely the primary resultant of the irradiation.

To the author's knowledge, this is the first execution of in situ measurement of radiation effects on piezoelectrically driven

© Published 2023. This article is a U.S. Government work and is in the public domain in the USA. Advanced Engineering Materials published by Wiley-VCH GmbH

15272648, 2023, 14, Downloaded from https://onlinelibrary.wiley.com/doi/10.1002/adem.202201837, Wiley Online Library on [18/07/2023]. See the Terms and Conditions (https://onlinelibrary.wiley.com/terms-and-conditions) on Wiley Online Library for rules of use; OA articles are governed by the applicable Creative Commons License

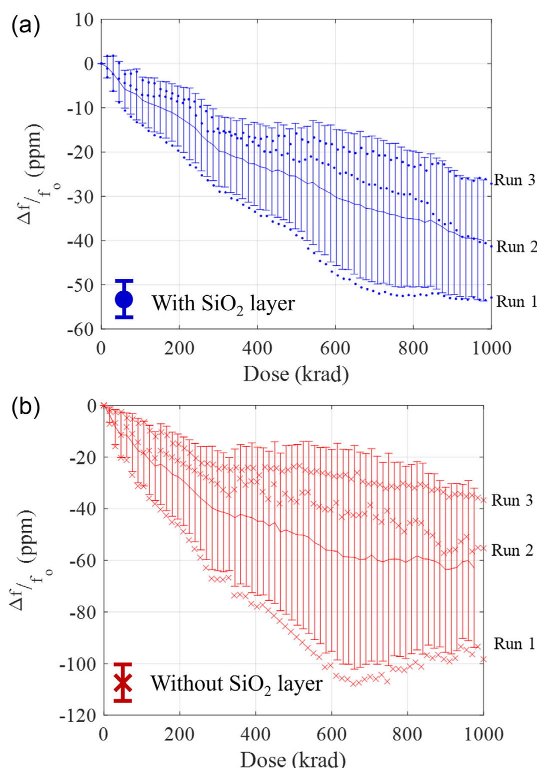

Figure 7. Statistical comparison between devices exposed to gamma rays. Shown are a) the device with the SiO_2 layer and b) the resonator without the oxide layer. Error bars are one standard deviation.

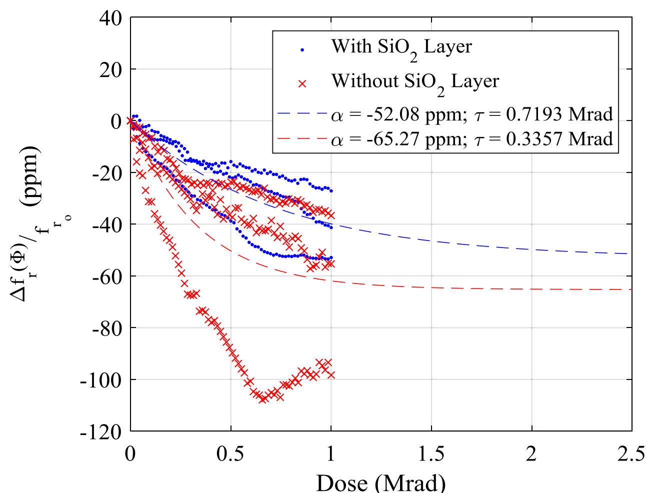

Figure 8. The fractional shift in resonant frequency data fits to the decaying exponential model. The decay constant (τ) is longer for the device with the added oxide layer.

Table 2. Resonator average acoustic velocity before and after 1 Mrad(Si) irradiation and corresponding theoretical shift in R_m.

Device	Average acoustic velocity [m s^{-1}]			ΔR_m [Ω]	
	Pre-Rad	Post rad	Δ	Theoretical	Measured
Without SiO_2	8,823.11	8,822.52	−0.59	−0.59	−7.71 ± 13.50
With SiO_2	8,893.46	8,893.11	−0.35	-0.35	8.32 ± 37.60

MEMS resonators. Very early research was not accomplished in situ and focused on the effects of charge build-up.[7,8,76] Displacement damage was only considered a significant effect once high-frequency RF MEMS emerged.[76] Polysilicon fixed-fixed beams irradiated to 16 krad(Si) exhibited a decrease in resonant frequency that was attributed to the relaxation of stress in the beams and not a change to Young's modulus.[77] Single-crystal AlN irradiated by fast and thermal neutrons and gamma rays up to 2.7 Grad exhibited no change to d_{33}.[75] An AlN single-crystal accelerometer was irradiated to 1.1 Mrad from a Co-60 source, with no significant degradation observed.[9] Most recently, an electrostatically driven comb drive resonator was irradiated by protons. A frequency shift of 298 ppm and a recovery of 189 ppm were measured.[78] By utilizing MEMS resonators operating in the VHF range, this work shows a detectable change in the effective Young's modulus of the material due to gamma irradiation. After a total dose of 1 Mrad(Si) Co-60 gammas, the average frequency shift ranged from 52 to 65 ppm with no recovery, and the change to the effective Young's modulus ranged from 104 to 131 ppm.

During the irradiation up to 1 Mrad, the resonant frequency shifts only a fraction of the device's bandwidth, and this shift remains stable at room temperature. This shift is much smaller than the precision obtainable by many commercial MEMS fabrication processes. Furthermore, the other resonator performance parameters – Q, R_m, and k^2_{eff} – remain stable throughout the irradiation. The stability of the resonator's Q, R_m, and one port k^2_{eff} demonstrates the resiliency of these devices in an ionizing radiation environment, providing a design space for systems engineers. Moreover, this experiment demonstrates the first use of gamma radiation to permanently trim the f_r of a resonator by up to 30% of its bandwidth without altering the device's other performance parameters.

3. Conclusion

The utility of MEMS devices in space and reactor systems necessitates research into how these devices behave in a radiation environment. Improvements to CMOS materials, novel design structures, and size reduction have made the devices inherently more resistant to most forms of radiation.[1] Therefore, it is vital to continue the study of radiation effects on other devices such as MEMS.

AlN transduced two-port rectangular flat plate resonators with and without a SiO_2 thin film were irradiated using Co-60 gammas. S-parameters were measured in situ while the devices were exposed to 1 Mrad(Si) at the OSU Co-60 Underwater Irradiator. The measured values of f_r, R_m, Q, and one port k^2_{eff} describe the device's reaction to TID effects. These measured values refine the theoretical model and identify radiation- and device-dependent damage and decay coefficients.

This work has demonstrated that these devices will experience a reduction in resonant frequency when placed in a gamma radiation environment up to 1 Mrad(Si). The frequency shift is due to

© Published 2023. This article is a U.S. Government work and is in the public domain in the USA. Advanced Engineering Materials published by Wiley-VCH GmbH

15272648, 2023, 14, Downloaded from https://onlinelibrary.wiley.com/doi/10.1002/adem.202201837, Wiley Online Library on [18/07/2023]. See the Terms and Conditions (https://onlinelibrary.wiley.com/terms-and-conditions) on Wiley Online Library for rules of use; OA articles are governed by the applicable Creative Commons License

high energy Compton electrons causing sufficient atomic displacement damage to alter the effective Young's modulus of the device. This effect is stable and does not change when the device is removed from the radiation environment and kept at room temperature. This work has also shown that these devices are largely immune to the effects of charge trapping, so R_m, Q, and k^2_{eff} remain relatively unaffected during gamma irradiation. The frequency shift due to gamma irradiation ranges from 10% to 30% of the device's bandwidth. The ability to shift the resonant frequency with gamma irradiation presents a new way of precise and permanent frequency trimming MEMS resonators without altering Q or other properties.

Additionally, adding the amorphous SiO_2 layer slows the frequency rate of change per unit dose of radiation. The reduction to the resonant frequency's sensitivity to gamma irradiation is captured in the time constant, τ, in that the addition of the SiO_2 thin film increases the τ of the resonator. Finally, this work demonstrates the usefulness of the modified diffusion model in describing the general change in the resonant frequency of a BAW resonator due to displacement damage. This model is a simple tool for predicting the behavior of a MEMS resonator subject to gamma ray or electron irradiation while preserving information about the material in the damage coefficients, α and τ. A key benefit is that this model does not need the high levels of computing power that a 3-dimensional molecular dynamics model would require.

These devices were exposed to a total ionizing dose of 1 Mrad(Si), similar to that experienced during the lifetime of a spacecraft. Engineering decisions such as shielding and device placement are essential when designing systems to operate in harsh radiation environments. Resiliency and an established relationship between radiation dose and device behavior provide a critical tool for the design process.

Supporting Information

Supporting Information is available from the Wiley Online Library or from the author.

Acknowledgements

The views expressed in this article are those of the authors and do not reflect the official policy or position of the United States Air Force, Department of Defense, or the US Government. The authors would like to acknowledge the support of The Ohio State University Nuclear Reactor Laboratory and the assistance of the reactor staff members, Kevin Herminghuysen, Andrew Kauffman, and Dr. Susan White, for the irradiation services provided. The authors would also like to thank the Air Force Research Labs (AFRL) Sensors Directorate for their support and Tim Prusnick for assisting with the Renishaw Raman Microscope, Dr. Matthew Hagedon for assisting with the laser dicing of the resonators, and Thomas Taylor for assisting with the wire bonding. Finally, the authors thank AFRL Materials and Manufacturing Directorate and the assistance of Dr. Derek Bas and Dr. Piyush Shah for their help with the PCB design.

Conflict of Interest

The authors declare no conflict of interest.

Data Availability Statement

The data that support the findings of this study are available from the corresponding author upon reasonable request.

Keywords

gamma-ray radiation, microelectromechanical resonators, piezoelectric resonators, radiation effects in electronics, radiation effects in MEMS

Received: December 18, 2022
Revised: May 14, 2023
Published online: June 19, 2023

[1] A. Holmes-Siedle, L. Adams, *Handbook of Radiation Effects*, Oxford University Press **2002**, https://global.oup.com/academic/product/handbook-of-radiation-effects-9780198507338?cc=us&lang=en&#
[2] J. R. Schwank, M. R. Shaneyfelt, P. E. Dodd, *IEEE Trans. Nucl. Sci.* **2013**, *60*, 2074.
[3] J. R. Schwank, M. R. Shaneyfelt, D. M. Fleetwood, J. A. Felix, P. E. Dodd, P. Paillet, V. Ferlet-Cavrois, *IEEE Trans. Nucl. Sci.* **2008**, *55*, 1833.
[4] H. R. Shea, *J. Micro/Nanolithogr. MEMS MOEMS* **2009**, *8*, 031303.
[5] J. R. Schwank, D. M. Fleetwood, *Appl. Phys. Lett.* **1988**, *53*, 770.
[6] N. S. Saks, M. G. Ancona, J. A. Modolo, *IEEE Trans. Nucl. Sci.* **1984**, *31*, 1249.
[7] N. F. de Rooij, S. Gautsch, D. Briand, C. Marxer, G. Mileti, W. Noell, H. Shea, U. Staufer, B. van der Schoot, in *Transducers*, IEEE, Denver, CO **2009**, pp. 17–24.
[8] J. Hales, M. Pedereson, in *16th Annual AIAA/USU Conf. Small Satellite* **2002**, https://digitalcommons.usu.edu/smallsat/2002/all2002/37/.
[9] C. I. Lee, A. H. Johnston, W. C. Tang, C. E. Barnes, *IEEE Trans. Nucl. Sci.* **1996**, *43*, 3127.
[10] A. R. Knudson, S. Buchner, P. McDonald, W. J. Stapor, A. B. Campbell, K. S. Grabowski, D. L. Knies, *IEEE Trans. Nucl. Sci.* **1996**, *43*, 3122.
[11] H. Kim, S. Kerrigan, M. Bourham, X. Jiang, *IEEE Trans. Ind. Electron.* **2021**, *68*, 534.
[12] D. Parrat, S. Gautsch, T. Akiyama, L. Howald, D. Brändlin-Müller, A. Tonin, H.-R. Hidber, M. Hecht, W. T. Pike, N. F. De Rooij, U. Staufer, in *Fourth Mars Polar Sci. Conf.* **2006**, https://citeseerx.ist.psu.edu/document?repid=rep1&type=pdf&doi=62432d1a71b8d881241c85ce62092e560ca5b645.
[13] Y. Wang, L. Qiu, Y. Luo, R. Ding, F. Jiang, *Mech. Syst. Signal Process* **2020**, *141*, 106730.
[14] M. Han, H. Wang, Y. Yang, C. Liang, W. Bai, Z. Yan, H. Li, Y. Xue, X. Wang, B. Akar, H. Zhao, H. Luan, J. Lim, I. Kandela, G. A. Ameer, Y. Zhang, Y. Huang, J. A. Rogers, *Nat. Electron.* **2019**, *6*, 26.
[15] G. Lee, D. Lee, J. Park, Y. Jang, M. Kim, J. Rho, *Commun. Phys.* **2022**, *5*, 94.
[16] H.-C. Song, S.-W. Kim, H. S. Kim, D.-G. Lee, C.-Y. Kang, S. Nahm, *Adv. Mater.* **2020**, *32*, 2002208.
[17] H. Chandrahalim, S. A. Bhave, R. G. Polcawich, J. Pulskamp, R. Kaul, *IEEE Electron. Device Lett.* **2009**, *30*, 1296.
[18] A. Gao, K. Liu, J. Liang, T. Wu, *Microsyst. Nanoeng.* **2020**, *6*, 74.
[19] L. Hackett, M. Miller, F. Brimigion, D. Dominguez, G. Peake, A. Tauke-Pedretti, S. Arterburn, T. A. Friedmann, M. Eichenfield, *Nat. Commun.* **2021**, *12*, 2769.
[20] A. Bashir, P. H. Wöbkenberg, J. Smith, J. M. Ball, G. Adamopoulos, D. D. C. Bradley, T. Anthopoulos, *Adv. Mater.* **2009**, *21*, 2226.

© Published 2023. This article is a U.S. Government work and is in the public domain in the USA. Advanced Engineering Materials published by Wiley-VCH GmbH

15272648, 2023, 14, Downloaded from https://onlinelibrary.wiley.com/doi/10.1002/adem.202201837, Wiley Online Library on [18/07/2023]. See the Terms and Conditions (https://onlinelibrary.wiley.com/terms-and-conditions) on Wiley Online Library for rules of use; OA articles are governed by the applicable Creative Commons License

[21] G. L. Smith, J. S. Pulskamp, L. M. Sanchez, D. M. Potrepka, R. M. Proie, T. G. Ivanov, R. Q. Rudy, W. D. Nothwang, S. S. Bedair, C. D. Meyer, R. G. Polcawich, *J. Am. Ceram. Soc.* **2012**, *95*, 1777.
[22] Q. Zhao, S. Liu, J. Chen, G. He, J. Di, L. Zhao, T. Su, M. Zhang, Z. Hou, *Rob. Auton. Syst.* **2021**, *140*, 103733.
[23] G. Pillai, S.-S. Li, *IEEE Sens. J.* **2021**, *21*, 12589.
[24] F. Maita, L. Maiolo, A. Minotti, A. Pecora, D. Ricci, G. Metta, G. Scandurra, G. Giusi, C. Ciofi, G. Fortunato, *IEEE Sens. J.* **2015**, *15*, 3819.
[25] J.-H. Park, D.-G. Jang, J. W. Park, S.-K. Youm, *Sensors* **2015**, *15*, 23402.
[26] C.-C. Chu, S. Dey, T.-Y. Liu, C.-C. Chen, S.-S. Li, *J. Microelectromech. Syst.* **2017**, *27*, 59.
[27] A. Rahafrooz, S. Pourkamali, *IEEE Trans. Electron Devices* **2012**, *59*, 3587.
[28] S. Bhattacharya, S.-S. Li, *IEEE Sens. J.* **2019**, *19*, 7261.
[29] T. L. Naing, T. O. Rocheleau, E. Alon, C. T. C. Nguyen, *IEEE Trans. Ultrason. Ferroelectr. Freq. Control* **2020**, *67*, 1377.
[30] J. R. Clark, W. Hsu, M. A. Abdelmoneum, C. T. Nguyen, *Perspective* **2005**, *14*, 1298.
[31] H. Chandrahalim, D. Weinstein, L. F. Cheow, S. A. Bhave, *Sens. Actuators, A* **2007**, *136*, 527.
[32] H. Chandrahalim, S. A. Bhave, E. Quevy, R. T. Howe, in *Int. Conf. Solid-State Sensors, Actuators Microsystems*, Lyon, France, June **2007**, pp. 313–316.
[33] H. Chandrahalim, S. A. Bhave, R. Polcawich, J. Pulskamp, D. Judy, R. Kaul, M. Dubey, in *Tech. Dig. - Solid-State Sensors, Actuators, Microsystems Work.* **2008**, p. 360, https://transducer-research-foundation.org/technical_digests/HiltonHead_2008/hh2008_0360.pdf.
[34] R. A. Johnson, *Mechanical Filters in Electronics*, John Wiley & Sons **1983**, https://www.amazon.com/Mechanical-Filters-Electronics-Wiley-filters/dp/0471089192/ref=sr_1_1?crid=2XUTX0H75UEFJ&keywords=Mechanical+Filters+in+Electronics+%28Wiley+Medical+Publication%29&qid=1685869263&sprefix=mechanical+filters+in+electronics+wiley+medical+publication+%2Caps%2C169&sr=8-1.
[35] S. Das, A. Kumar, A. Kumar, J. Singh, R. Jha, M. Kumar, *IEEE Trans. Electron Devices* **2021**, *68*, 2791.
[36] X. Bian, H. Jin, X. Wang, S. Dong, G. Chen, J. K. Luo, M. J. Deen, B. Qi, *Sci. Rep.* **2015**, *5*, 9123.
[37] M. Hodjat-Shamami, F. Ayazi, *Microsyst. Nanoeng.* **2020**, *6*, 108.
[38] K. Obitani, K. Araya, M. Yachi, T. Tsuchiya, *J. Microelectromech. Syst.* **2021**, *30*, 384.
[39] S. Shin, A. Daruwalla, M. Gong, H. Wen, F. Ayazi, in *2019 20th Int. Conf. Solid-State Sensors, Actuators and Microsystems & Eurosensors XXXIII (Transducers & Eurosensors XXXIII)*, Berlin, Germany, June **2019**, pp. 503–506.
[40] H. Mansoorzare, A. Todi, S. Moradian, R. Abdolvand, *2020 IEEE Int. Ultrasonics Symp.*, Las Vegas, NV, September **2020**, p. 1.
[41] H. Chandrahalim, S. A. Bhave, in *Proc. IEEE Int. Conf. Micro Electro Mechanical Systems*, Tucson, AZ, January **2008**, p. 1020.
[42] H. Chandrahalim, S. A. Bhave, R. G. Polcawich, J. S. Pulskamp, R. Kaul, *IEEE Trans. Ultrason. Ferroelectr. Freq. Control* **2010**, *57*, 2035.
[43] D. Chen, H. Zhang, J. Sun, M. Pandit, G. Sobreviela, Y. Wang, Q. Zhang, X. Chen, A. Seshia, J. Xie, *Phys. Rev. Appl.* **2020**, *14*, 014001.
[44] R. Lu, S. Gong, *J. Micromech. Microeng.* **2021**, *31*, 114001.
[45] S. Rassay, D. Mo, C. Li, N. Choudhary, C. Forgey, R. Tabrizian, *IEEE Electron Device Lett.* **2021**, *42*, 1065.
[46] A. Ansari, M. Rais-Zadeh, *IEEE Electron Device Lett.* **2014**, *35*, 1127.
[47] G. Piazza, P. J. Stephanou, A. P. Pisano, *J. Microelectromech. Syst.* **2007**, *16*, 319.
[48] H. Bhugra, G. Piazza, *Piezoelectric MEMS Resonators*, Springer International Publishing, Cham **2017**.
[49] R. M. R. Pinto, V. Gund, R. A. Dias, K. K. Nagaraja, K. B. Vinayakumar, *J. Microelectromech. Syst.* **2022**, *31*, 500.
[50] T. Furukawa, K. Ishida, E. Fukada, *J. Appl. Phys.* **1979**, *50*, 4904.
[51] R. T. Smith, F. S. Welsh, *J. Appl. Phys.* **1971**, *42*, 2219.
[52] T. Yamada, N. Niizeki, H. Toyoda, *Jpn. J. Appl. Phys.* **1967**, *6*, 151.
[53] F. Xu, S. Trolier-McKinstry, W. Ren, B. Xu, Z.-L. Xie, K. J. Hemker, *J. Appl. Phys.* **2001**, *89*, 1336.
[54] V. V. Felmetsger, P. N. Laptev, R. J. Graham, *J. Vac. Sci. Technol., A, Vac., Surf., Film.* **2011**, *29*, 021014.
[55] S. Shahraini, H. Mansoorzare, A. Mahigir, R. Abdolvand, *J. Microelectromech. Syst.* **2020**, *29*, 296.
[56] C. Fei, X. Liu, B. Zhu, D. Li, X. Yang, Y. Yang, Q. Zhou, *Nano Energy* **2018**, *51*, 146.
[57] G. Piazza, V. Felmetsger, P. Muralt, R. H. I. Olsson, R. Ruby, *MRS Bull.* **2012**, *37*, 1051.
[58] M. A. Xapsos, G. P. Summers, C. C. Blatchley, C. W. Colerico, E. A. Burke, S. R. Messenger, P. Shapiro, *IEEE Trans. Nucl. Sci.* **1994**, *41*, 1945.
[59] D. M. Fleetwood, *IEEE Trans. Nucl. Sci.* **1997**, *44*, 1826.
[60] D. M. Fleetwood, P. S. Winokur, M. R. Shaneyfelt, L. C. Riewe, O. Flament, P. Paillet, J. L. Leray, in *Effects of Irradiation and Isochronal Anneal Temperature on Hole and Electron Trapping in MOS Devices* **1998**, https://www.osti.gov/biblio/645591.
[61] H. Y. Tada, J. R. Carter, B. E. Anspaugh, R. G. Downing, *Solar Cell Radiation Handbook: Third Edition* **1982**.
[62] G. P. Summers, E. A. Burke, P. Shapiro, S. R. Messenger, R. J. Walters, *IEEE Trans. Nucl. Sci.* **1993**, *40*, 1372.
[63] G. W. Kinchin, R. S. Pease, *Rep. Prog. Phys.* **1955**, *18*, 1.
[64] L. B. Freund, S. Suresh, *Thin Film Materials: Stress, Defect Formation and Surface Evolution*, Cambridge University Press **2004**, https://doi.org/10.1017/CBO9780511754715.
[65] M. A. Hopcroft, W. D. Nix, T. W. Kenny, *J. Microelectromech. Syst.* **2010**, *19*, 229.
[66] J. S. Custer, M. O. Thompson, D. C. Jacobson, J. M. Poate, S. Roorda, W. C. Sinke, F. Spaepen, *Appl. Phys. Lett.* **1994**, *64*, 437.
[67] M. Polińska, A. Rozanski, A. Galeski, J. Bojda, *Macromolecules* **2021**, *54*, 9113.
[68] J. Hessinger, B. E. White, R. O. Pohl, *Planet. Space Sci.* **1996**, *44*, 937.
[69] H. Chandrahalim, S. A. Bhave, R. G. Polcawich, J. S. Pulskamp, R. Kaul, in *Proc. - IEEE Ultrason. Symp.* **2009**, p. 2145.
[70] D. D. Lynes, H. Chandrahalim, *Adv. Mater. Interfaces* **2023**, *10*, 2202446.
[71] K. Hashimoto, in *Piezoelectric MEMS Resonators* (Eds: H. Bhugra, G. Piazza), Springer International Publishing, Cham **2017**.
[72] W. Chen, W. Jia, Y. Xiao, G. Wu, *J. Microelectromech. Syst.* **2022**, *31*, 318.
[73] Z. Wu, A. Peczalski, V. A. Thakar, Z. Cao, Y. Yuan, G. He, R. L. Peterson, K. Najafi, M. Rais-Zadeh, in *Proc. IEEE Int. Conf. on Micro Electro Mechanical Systems*, Taipei, Taiwan, January **2013**, p. 122.
[74] D. C. Montgomery, *Design and Analysis of Experiments*, John Wiley & Sons, Inc **2013**, ISBN-10: 8126540508, ISBN-13: 978-8126540501.
[75] D. Parks, B. Tittmann, *IEEE Trans. Ultrason. Ferroelectr. Freq. Control* **2014**, *61*, 1216.
[76] H. R. Shea, *Reliab. Packag. Tes. Charact. MEMS/MOEMS Nanodevices X* **2011**, *7928*, 79280E.
[77] L. Wang, Q. A. Huang, J. Tang, J. Luo, in *Proc. Int. Symp. on the Physical and Failure Analysis of Integrated Circuits, IPFA*, Suzhou, China, July **2009**, p. 764.
[78] J. Lee, M. W. McCurdy, R. A. Reed, R. D. Schrimpf, M. A. Alles, P. X.-L. Feng, *IEEE Trans. Nucl. Sci.* **2023**, *70*, 462.

 © Published 2023. This article is a U.S. Government work and is in the public domain in the USA. Advanced Engineering Materials published by Wiley-VCH GmbH

15272648, 2023, 14, Downloaded from https://onlinelibrary.wiley.com/doi/10.1002/adem.202201837, Wiley Online Library on [18/07/2023]. See the Terms and Conditions (https://onlinelibrary.wiley.com/terms-and-conditions) on Wiley Online Library for rules of use; OA articles are governed by the applicable Creative Commons License

Supporting Information

Effects of gamma ray radiation on the performance of microelectromechanical resonators

David D. Lynes[1,*], Hengky Chandrahalim[1,*], James E. Bevins[2], and James C. Petrosky[2]

[1] Department of Electrical and Computer Engineering

[2] Department of Engineering Physics

Air Force Institute of Technology,

Wright-Patterson Air Force Base, OH 45433, USA

*Corresponding Authors:

david.lynes.2@au.af.edu

hengky@microsystems.group

S.1 Fabrication

The resonator designs are fabricated using the PiezoMUMPs process by MEMSCap.[1] The fabrication design flow is presented in Figure S2. The substrate is a 150 mm (100) oriented silicon-on-insulator (SOI) wafer. Phosphorus is used to n-dope the silicon layer to increase conductivity. A thermal oxide layer is grown and wet etched. The AlN film is deposited using reactive sputtering and is then wet etched. Next, 20 nm chromium and 1000 nm Al are deposited and patterned by a lift-off process. The n-Si and SiO_2 layers are lithographically patterned and etched by reactive ion etching (RIE). Finally, the devices are released via a back-etch of the handle wafer by a combination of RIE and wet etch.[1]

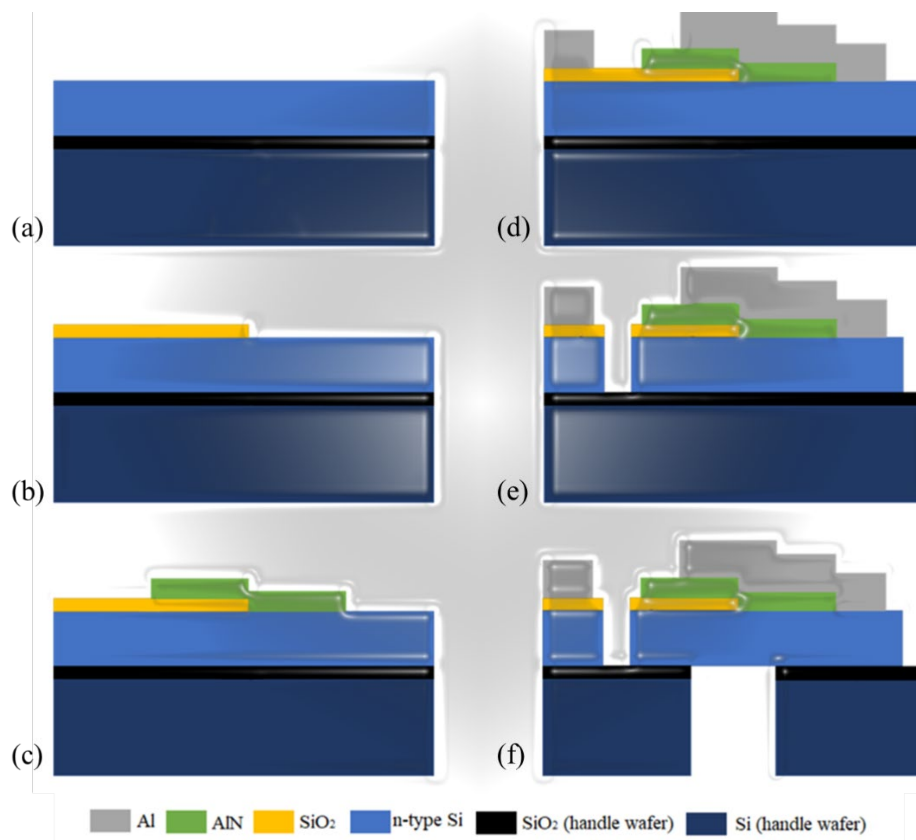

Figure S1. Summary of PiezoMUMPs fabrication process flow. (a) Top Si layer of SOI wafer is n-doped. (b) Patterning of thermal oxide layer. (c) Deposition and patterning of AlN. (d) Deposition and patterning of Al layer. (e) RIE of oxide and n-Si. (f) Backside RIE of handle wafer.

S.2 Raman Spectroscopy

Raman spectra were collected on the surface silicon before and after irradiation using a 532 nm excitation laser. The samples were prepared using a 30 second acetone rinse, 30 sec methanol rinse, 30 sec isopropanol rinse, and blown dry with nitrogen. Crystalline silicon has a sharp peak at 521 cm^{-1}. As silicon becomes amorphous, a broad band appears in the Raman spectra centered at 480 cm^{-1}.[2] The ratio between the peaks is used to estimate the relative amount of amorphous material. Figure S2 presents the Raman spectra of the surface silicon. No peak at 480 cm^{-1} is present, nor has the peak at 521 cm^{-1} experienced any significant reduction in magnitude. Together, these indicate the silicon has retained a majority of its crystallinity. This is reasonable in that the gamma ray irradiation interacts uniformly throughout the material and the atomic defect density is roughly 1 in 6.5×10^8 atoms.

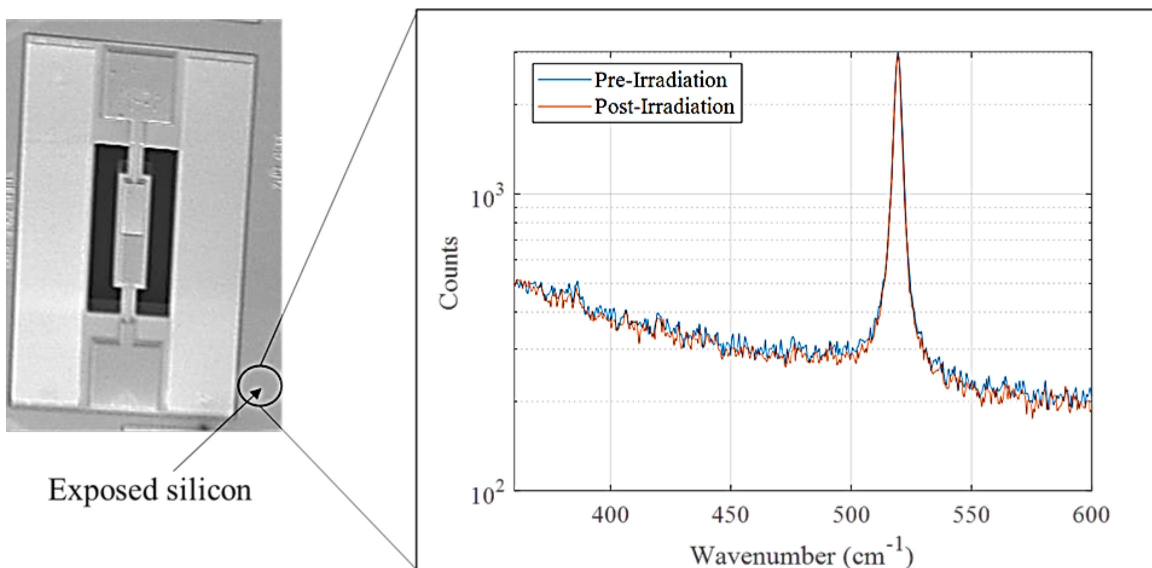

Figure S2. Raman spectra of surface silicon before and after 1 Mrad gamma ray exposure.

S.3 Tabulated Results

Table S1 presents the measured pre- and post- irradiation resonator parameter values f_r, Q, R_m, and k_{eff}^2. Table S1 presents the change in device parameters after a 15-minute room temperature timed anneal.

Table S1. Measured pre- and post-irradiation resonator parameters.

Run #	With SiO2 Layer?	f_r (MHz)			Q			R_m (Ω)			k_{eff}^2 (%)		
		Pre-Rad	Post-Rad	Δ	Pre-Rad	Post-Rad	Δ	Pre-Rad	Post-Rad	Δ	Pre-Rad	Post-Rad	Δ
1	No	78.7379	78.7298	-0.0081	1944.52	1951.91	7.39	1740.12	1729.67	-10.45	0.101402	0.100687	-0.000715
2	No	78.9056	78.9011	-0.0045	1914.01	1897.93	-16.08	1816.1	1823.05	6.95	0.105627	0.105677	5E-05
3	No	78.6895	78.6866	-0.0029	2231.03	2257.85	26.82	1483.52	1463.9	-19.62	0.087854	0.0873779	-0.000476
1	Yes	71.5831	71.5792	-0.0039	4895.89	4928	32.11	4327.98	4295.31	-32.67	0.0404843	0.0401373	-0.000347
2	Yes	71.8467	71.8437	-0.003	4513.25	4467.26	-45.99	4725.51	4766.71	41.2	0.0443568	0.0439127	-0.000444
3	Yes	71.7349	71.7327	-0.0022	7059.6	7017.24	-42.36	2872.11	2888.55	16.44	0.028093	0.028187	9.4E-05

Table S2. Measured resonator parameters pre- and post- 15-minute room temperature anneal.

Run #	With SiO2 Layer?	f_r			Q			R_m			k_{eff}^2		
		$\Delta_{0\ min}$	$\Delta_{15\ min}$	Rebound	$\Delta_{0\ min}$	$\Delta_{15\ min}$	Rebound	$\Delta_{0\ min}$	$\Delta_{15\ min}$	Rebound	$\Delta_{0\ min}$	$\Delta_{15\ min}$	Rebound
1	No	-0.0081	-0.0088	-0.0007	7.39	2.88	-4.51	-10.45	-9.9	0.55	-0.000715	0.0905754	0.0912904
2	No	-0.0045	-0.0088	-0.0043	-16.08	-34.51	-18.43	6.95	16.63	9.68	5E-05	0.001471	0.001421
3	No	-0.0029	-0.0021	0.0008	26.82	50.62	23.8	-19.62	-38.1	-18.48	-0.000476	-0.0015687	-0.0010927
1	Yes	-0.0039	-0.0077	-0.0038	32.11	82.29	50.18	-32.67	-68.06	-35.39	-0.000347	-0.0009171	-0.0005701
2	Yes	-0.003	-0.0068	-0.0038	-45.99	-75.19	-29.2	41.2	73.08	31.88	-0.000444	0.0004561	0.0009001
3	Yes	-0.0022	-0.0012	0.001	-42.36	-94.03	-51.67	16.44	19.62	3.18	9.4E-05	6.33E-05	-0.0000307

References

[1] A. Cowen, G. Hames, K. Glukh, B. Hardy, *MEMSCAP Inc* **2014**, *1*.

[2] T. Deschaines, J. Hodkiewicz, P. Henson, *Thermo Sci.* **2009**, 3.